I&EC research
Industrial & Engineering Chemistry Research

Article

Cite This: Ind. Eng. Chem. Res. XXXX, XXX, XXX−XXX

pubs.acs.org/IECR

Solid-State Conversion of Scandium Phosphate into Scandium Oxide with Sodium Compounds

Bengi Yagmurlu,*[,†,‡,⊥] Wenzhong Zhang,[§,⊥] Mikko J. Heikkilä,[∥] Risto T. Koivula,[§] and Bernd Friedrich[‡]

[†]MEAB Chemie Technik GmbH, 52068 Aachen, Germany
[‡]IME Institute of Process Metallurgy and Metal Recycling, RWTH Aachen University, 52056 Aachen, Germany
[§]Department of Chemistry—Radiochemistry, University of Helsinki, P.O. Box 55, FI-00014 Helsinki, Finland
[∥]Department of Chemistry, University of Helsinki, P.O. Box 55, FI-00014 Helsinki, Finland

Supporting Information

ABSTRACT: The application of scandium (Sc) is hindered by insufficient supply. The majority of the world Sc supply is sourced from industrial byproducts, where Sc needs to be separated from other components. Phosphate precipitation is an effective separation and purification method to harvest dissolved Sc ions from acidic leachate solutions; however the obtained Sc phosphate currently has no direct application. To this end, a solid-state conversion route of Sc phosphate to oxide was investigated by using five different sodium compounds, as sodium forms very stable phosphate compounds. The thermal conversion (up to 1000 °C) of Sc phosphate with high melting point sodium compounds (sodium sulfate, carbonate, and chloride) yielded a stable mixed sodium−scandium phosphate phase with a formula of $Na_3Sc_2(PO_4)_3$. The thermal conversion with lower melting point sodium compounds (sodium hydroxide and nitrate) resulted in the separation of Sc from phosphate moieties, forming respectively Sc oxides ($NaScO_2$ or Sc_2O_3) and sodium phosphate. In situ high temperature X-ray diffraction, differential scanning calorimetry (DSC), and thermogravimetry (TGA) were employed to investigate the solid-state conversion process by sodium nitrate. Slower heating rate (120 °C/h) and the evolution of oxygen gas (as a result of sodium nitrate decomposition) favored the formation of Sc_2O_3 phase over $NaScO_2$ phase, and the conversion reaction was completed at 670 °C. The conversion process was further explored as a purification step toward Sc-containing mixed phosphate precipitates, where the impurities (aluminum and iron phosphates) were converted into sodium aluminate and ferrite and could then be separated from Sc_2O_3 by their differences in acid/base solubility.

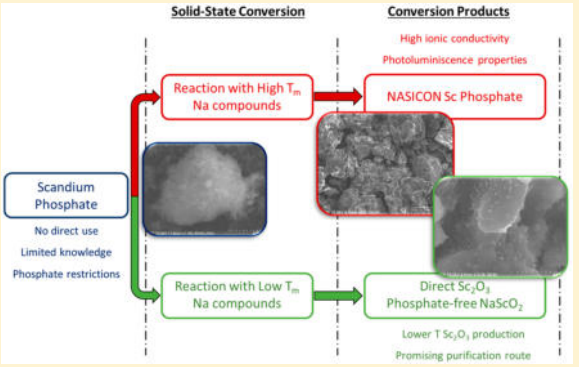

1. INTRODUCTION

Recent climate accords and subsequent legislations have specified the deadlines for the automotive industry to reduce carbon emission in an effort to combat global warming.[1] This has placed light metals and alloys under the spotlight. The predominant reason is the direct relation between vehicle weight and its energy consumption. Scandium (Sc) is used as a tuning metal for aluminum alloys, making it one of the most promising candidates for lightweight alloys. Minor additions of Sc provide aluminum alloys with improved strength, thermal resistance, and weldability.[2−5] Another important application of Sc is in solid-oxide fuel cells, where Sc attains improved oxygen-ion conductivity.[6−8] Sc is, however, an extremely expensive metal for mass application in industrial usage. According to Stanford Materials, the price of Sc metal currently stands at approximately 5 USD per gram.[9] The annual worldwide Sc production and consumption are estimated to be 10−15 metric tonnes (in the form of Sc_2O_3) by the U.S. Geological Survey.[9] Hence, Sc was classified as a critical metal for the future, owing to the steep increase in demand despite its current price.[10]

Since Sc is widely dispersed in low concentration in the nature, it is recovered almost only as a byproduct of uranium, nickel laterite, titanium pigment processing, and recently bauxite residue valorisation.[11−14] Many efforts were given to recover Sc from these secondary resources, and different processes were proposed, especially in laboratory scale.[15−17] Some of the newly developed novel processes to separate Sc from the impurities, i.e., selective precipitation, inorganic metal phosphates, supported ionic liquid phases, etc., offer good recovery rates as well as selectivity.[18−22] However, a majority of those novel processes have limitations because of the

Received: May 2, 2019
Revised: July 13, 2019
Accepted: July 16, 2019
Published: July 16, 2019

DOI: 10.1021/acs.iecr.9b02411
Ind. Eng. Chem. Res. XXXX, XXX, XXX−XXX

operation parameters used and have only been carried out in smaller scale.

In our previous studies, we presented a novel selective precipitation route to refine a Sc concentrate from different leachates with a potential to adapt into larger scale operations.[18,23] In this process, the main interfering impurity in recoverable Sc feed solutions, Fe, is separated in dual-step Fe removal stages, which is then successively followed by a one-stage phosphate precipitation step to selectively remove Sc as phosphate. The final major impurity in the Sc concentrate is Al. Furthermore, recently developed Sc recovery operations from secondary resources also consist of at least one step utilizing phosphoric acid during processing, which might result in the formation of the scandium phosphate during further treatment.[21,22]

However, the product obtained from this precipitation process is a type of Sc phosphate that does not currently have a known application area at the moment. In addition, very limited literature is available about the nature and properties of any Sc phosphate compounds.[24,25] Hence, this Sc concentrate needs to be converted into a Sc compound, i.e., Sc_2O_3, which has a higher demand from the end users. Moreover, phosphate compounds have more strict regulations, during both synthesis and operation stage. For this purpose, in this paper, the Sc phosphate precipitates, produced by a dibasic phosphate precipitation route, were converted into different scandium compounds by solid-state reactions. Since sodium (Na) forms thermodynamically highly stable phosphate compounds, different Na compounds were selected to aid the conversion. The conversion from Sc phosphate into Sc oxide or mixed oxide also eliminates the phosphorus-containing moieties, thereby favoring the further processing and purification. The behavior of main impurities (i.e., Fe^{3+} and Al^{3+}) during the conversion was also examined.

2. EXPERIMENTAL SECTION

2.1. Preparation of Metal Phosphates. The metal phosphates (MeP) were obtained by a precipitation reaction. To a 1 M solution of pure metal sulfate, a 1 M ammonium dihydrogen phosphate ($NH_4H_2PO_4$) solution was added dropwise under magnetic stirring (200 rpm) until the solution pH reached 2.0 ± 0.1. The precipitated slurry was paper-filtered and washed three times with water to remove the residual soluble sulfate and phosphate. The phosphate salts were dried in an oven at 105 °C overnight and kept in a desiccator. Scandium phosphate (ScP) and iron phosphate (FeP) were prepared in this manner.

2.2. Conversion of MeP by Sodium Compounds. MeP was mixed and ground together with a stoichiometric amount of sodium compounds [including NaOH (0.86 g/g of ScP), NaCl (1.23 g/g of ScP), Na_2CO_3 (1.13 g/g of ScP), $NaNO_3$ (1.96 g/g of ScP), and Na_2SO_4 (1.53 g/g of ScP)] using a mortar and pestle and then transferred to a ceramic crucible. The composition of MeP was assumed to be $MePO_4$ for easier calculation. The conversion of MeP was done by heating the reaction mixture under atmospheric conditions at two different heating rates, reaching respectively 300, 350, 750, and 900 °C and held there for 1 h in a Nabertherm L 3/12 muffle furnace. The temperature intervals were selected based on the melting points and decomposition temperatures of the sodium compounds used. Two sets of experiments were conducted, one with rapid heating (1000 °C/h) and another one with slower heating rate (120 °C/h).

2.3. Conversion of the Industrially Sourced Mixed Phosphate. The proposed solid-state conversion protocol was validated by a mixed phosphate sample sourced from industrial processes. Sc-containing Greek bauxite residue was smelted together with lime as a fluxing agent to remove the Fe in the bauxite residue via carbothermic reduction and to control the slag minerology.[26,27] Then, the synthesized slag was removed from the metal part (pig iron) and milled to obtain finer particles. Slag which is concentrated in terms of Sc was leached by sulfuric acid−hydrogen peroxide mixture.[28] Impurity removal of the pregnant leach solution (PLS) was done by the addition of NH_4OH which is followed by selective Sc precipitation by dibasic phosphate.[22,23,29] The formed mixed phosphate was dried under 60 °C in an oven, and its metal composition is listed in Table 1. The conversion was carried out by the same procedure as mentioned earlier using an excess amount of $NaNO_3$ (by assuming the stoichiometric amount of converting pure $AlPO_4$) and a heating rate of 120 °C/h. The conversion temperature was chosen to be 750 °C, and the reaction mixture was held at the temperature for 1 h after the controlled heating.

Table 1. Content of the Phosphate Mixture Synthesized from Bauxite Residue

	Si	Ti	Ca	Al	Fe	Sc
content (wt %)	0.81	0.46	0.21	6.42	0.37	0.018
SD (%)	0.05	0.02	0.01	0.07	0.01	0.001

2.4. Dissolution of the Converted Oxide. The dissolution of the converted oxide was tested sequentially in base and acid solutions. Approximately 100 mg of the converted oxide was placed into a polyethylene bottle, and 10 mL of 1 M NaOH solution was added. The bottle was rotary mixed (50 rpm) for 5 min before centrifugation at 2000*g*. Thereafter, exactly 9.5 mL of the supernatant was taken out for metal analysis, and 9.5 mL of fresh acid/base solution was added to continue the dissolution cycles in a same manner. Altogether 10 cycles were performed, with the first six cycles using 1 M NaOH and the final four cycles using 1 M HNO_3.

The dissolution percentage of the first cycle (D_1) is calculated by

$$D_1\ (\%) = \frac{c_1 10}{C} \times 100 \tag{1}$$

where c_1 is the elemental concentration (mg/L) in the 10 mL leaching solution and C is the elemental content in the converted solid (μg).

From the second cycle onward, the dissolution percentage is calculated by

$$D_n\ (\%) = \frac{c_n 10 - c_{n-1} 0.5}{C} \times 100 \tag{2}$$

where D_n is the dissolution percentage of cycle n, c_n is the elemental concentration measured from the solution taken out from the cycle n, and c_n is the elemental concentration measured from the solution in the previous cycle.

2.5. Characterization Methods. Powder X-ray diffraction (XRD) patterns were collected using a PANalytical X'Pert PW3710 MPD diffractometer coupled with a PW3020 vertical goniometer in Bragg−Brentano geometry. X-ray radiation was sourced from monochromatic Cu Kα line (λ = 1.540 56 Å) operating at 40 kV and 40 mA.

DOI: 10.1021/acs.iecr.9b02411
Ind. Eng. Chem. Res. XXXX, XXX, XXX−XXX

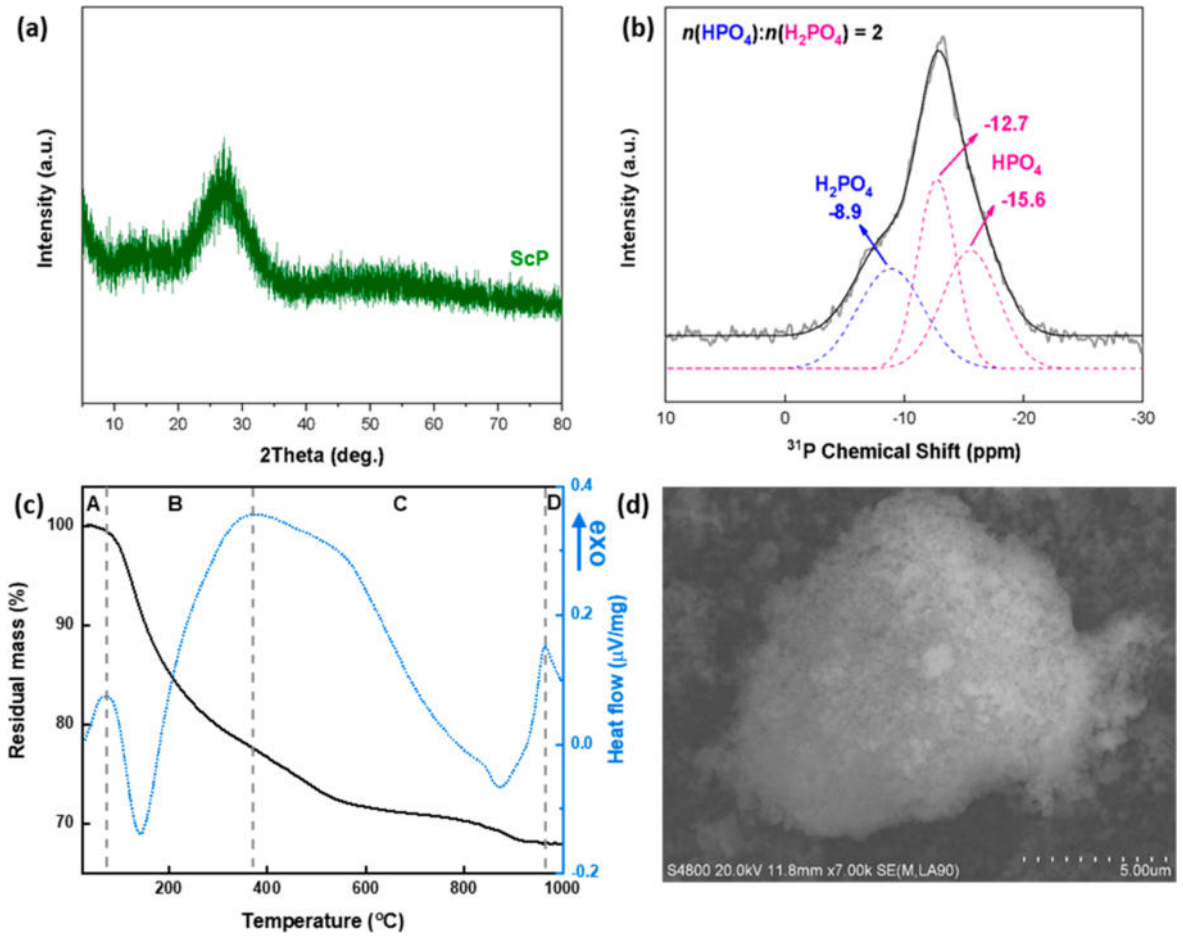

Figure 1. Structural characterizations of the ScP by powder XRD (a), solid-state ^{31}P MAS NMR (b), and DTA-DSC (c). The SEM micrograph of the ScP is shown in (d).

High-temperature XRD patterns were measured using a PANalytical X'Pert Pro MPD diffractometer with an attached Anton Paar HTK-1200 N furnace. The measurements were done in air in the temperature range of 25−1000 °C, first at 25 °C and second at 250 °C, and then progressing to 1000 °C in 15 °C intervals, after which the sample was cooled and final measurement performed at 25 °C. Each measurement took approximately 10 min. Phase identification was based on ICDD PDF cards: 00-031-1318 cubic Na_3PO_4, 5-629 cubic Sc_2O_3, 18-1232 rhombohedral $NaScO_2$, and 46-1212 rhombohedral Al_2O_3 (corundum).

The differential scanning calorimetry (DSC) and thermogravimetry (TGA) thermograms were collected from 30 mg of specimen by NETZSCH simultaneous thermal analyzer (STA) 449 F3 Jupiter with SiC furnace and a heating rate of 10 °C/min under constant Ar flow.

The morphology and local composition of the products were examined using a Hitachi S-4800 FE-SEM (field-emission scanning electron microscopy) coupled with an Oxford INCA 350 Energy spectrometer, after coating with a 3 nm layer of Pd−Au by sputtering.

Solid-state ^{31}P magic-angle spinning nuclear magnetic resonance (MAS NMR) spectra were obtained with a Bruker Avance III NMR spectrometer operating at 500 MHz for protons. Scandium phosphate was packed in a 4 mm zirconia rotor and spun at a frequency of 12 kHz. Spectra were acquired using 7.22 μs pulse and 5 s recycle delay and were externally referenced to 85% H_3PO_4 at 0 ppm.

Metal concentrations were measured on an Agilent microwave plasma atomic emission spectrometer (MP-AES) 4200 using standard calibration methods. Samples were diluted into the concentration range between 0 and 10 mg L^{-1} before analysis.

3. RESULTS AND DISCUSSION

3.1. Characterization of the ScP Precipitates. The ScP was prepared by first dissolving $Sc_2(SO_4)_3$ in deionized water until a clear solution is obtained and then precipitating it via the addition of dibasic phosphates, in this case $(NH_4)_2HPO_4$ in order not to contaminate the precipitate with ions such as Na^+ or K^+. Since there is very limited study and knowledge regarding Sc and phosphate speciation, the structure and properties of the precipitated ScP were extensively characterized.

The crystal structure of the synthesized ScP precipitate was characterized by XRD. The XRD diffractogram (in Figure 1a) shows a wide hump between 20° and 40° 2θ, indicating an amorphous or nanocrystalline structure. To the best of our knowledge, no information regarding the composition of amorphous ScP can be found in the literature. Therefore, the nature of the phosphate moiety was examined by solid-state ^{31}P MAS NMR. A broad resonance peak centered at −12.7 ppm is observed from the spectrum (Figure 1b), which is

DOI: 10.1021/acs.iecr.9b02411
Ind. Eng. Chem. Res. XXXX, XXX, XXX−XXX

typical for amorphous materials since the local environment for P differs. The broad peak can be deconvoluted into three peaks: one at −8.9 ppm, another at −12.7 ppm, and the third at −15.6 ppm. The first peak represents H_2PO_4 group, while the last two signify HPO_4 groups.[30] The estimated molar ratio of HPO_4-to-H_2PO_4 groups is 2, based on the area of the deconvoluted peaks. According to the digestion results, the ratio of Sc/P is 0.597 ± 0.003. We selected an approximate ratio of 3:5 for further calculations. Combined with all the characterization methods, the formula of the precipitated ScP is identified as $Sc_9(HPO_4)_{10}(H_2PO_4)_5(OH)_2{\cdot}27H_2O$. The phosphate precipitation was carried out until the solution pH attained 2.0, and at that pH, most of phosphate speciation should be undissociated phosphoric acid and $H_2PO_4^-$ (the pK_{a1} of phosphoric acid is 2.15). The presence of hydroxyl groups and HPO_4 groups in the precipitated ScP should result from a high local pH during the addition of ammonium dihydrogen phosphate.

Figure 1c shows the thermal behavior of the ScP precipitate upon heating. Four different stages of transformation (denoted as A, B, C, and D on the graph) were observed during heating from room temperature to 1000 °C. In regions A and B, unbound and crystal water which comprised approximately 20% of the total mass was evaporated from the precipitate. As the temperature of the system continued to increase, the condensation of HPO_4, H_2PO_4, and OH groups with a loss of 7% of the initial mass was observed within a wide temperature range between 375 and 975 °C, region C. The precipitate then started a pyrophosphate transformation in region D. The SEM micrographs of the amorphous ScP precipitates were given in Figure 1d. This amorphous ScP precipitate consisting of homogeneously dispersed very fine, irregularly shaped porous particles which can be seen from the micrograph.

Phosphate precipitation of Sc from aqueous solutions is a promising option to recover Sc from various resources since this precipitation step is highly selective toward Sc.[23] However, the product ScP has no known usage in the industry, and since it contains a phosphate group, the regulations toward this kind of product are stricter. To convert ScP into a preferred product as well as minimize the phosphate moiety, Na compounds are selected as the best candidates because of the high stability of Na phosphates. Thus, various Na compounds, NaOH, NaCl, Na_2SO_4, Na_2CO_3, and $NaNO_3$, were reacted with ScP precipitate at different temperatures.

3.2. Solid State Interaction between ScP and High T_m Na Compounds (NaCl, Na_2SO_4, and Na_2CO_3). In order to initiate a solid-state reaction between Na compounds and ScP and convert ScP into another compound without a phosphate group, first the Na compounds with higher T_m were investigated. For this purpose, NaCl, Na_2SO_4, and Na_2CO_3 were selected as the candidates for the conversion process since their melting or decomposition temperatures are similar. As it can be seen from the equations below, while NaCl melts at 801 °C, Na2SO4 melts at 884 °C and Na_2CO_3 undergoes a decomposition at 854 °C, yielding Na_2O and CO_2.

$$NaCl(s) \xrightarrow{801\,^\circ C} NaCl(l) \quad (3)$$

$$Na_2SO_4(s) \xrightarrow{884\,^\circ C} Na_2SO_4 \quad (4)$$

$$Na_2CO_3(s) \xrightarrow{854\,^\circ C} Na_2O(s) + CO_2(g) \quad (5)$$

The aim is to remove the phosphate moiety from ScP by reacting these compounds to yield either NaSc-based oxide or another Sc compound and Na_3PO_4 as a result of reaction in a furnace. Although highly stable salts such as NaCl or Na_2SO_4 might not react with ScP and might be an unsuccessful trial to remove phosphate from ScP, lack of thermodynamic data especially about Sc, intention to observe and compare the behaviors of similar salts, and unpredictable reactions in salt melts were the major foundations of these investigations.

The XRD diffractograms of the solids obtained after reacting high T_m Na compounds with ScP at various temperatures could be seen in Figure 2. No reaction between ScP and NaCl was observed at 300 °C, and only NaCl peaks were observed in the diffractogram. As the temperature increased to 750 °C, partial formation of $Na_3Sc_2(PO_4)_3$ was observed as a result of diffusion since the mixture was mixed together with fine grinding, consequently forming a diffusion couple. Formation of a more $Na_3Sc_2(PO_4)_3$ phase was noted as a result of increasing the ambient temperature to 900 °C since the diffusion between these two particles was accelerated at elevated temperatures. However, upon increase in the temperature, instead of forming stable Na_3PO_4 by the exchange of PO_4, amorphous ScP takes Na from ionic NaCl melt to form monoclinic $Na_3Sc_2(PO_4)_3$. Hence, the phosphate moiety could not be removed from ScP. A similar behavior was also observed in the case of Na_2SO_4. It can be seen from Figure 2b that rather than diffusion of phosphate into Na compound, Na was diffused into ScP to form $Na_3Sc_2(PO_4)_3$.

Although the behavior is comparable to NaCl and Na_2SO_4 until 750 °C, partial transformation of ScP was observed when ScP was reacted with Na_2CO_3 at 900 °C which is presented in Figure 2c. The phases presented after reacting ScP with Na_2CO_3 at 900 °C were found as Na_3PO_4, $NaScO_2$, and $Na_3Sc_2(PO_4)_3$. These phases are the indicators that a partly successful transformation of ScP into phosphate-free Sc compound could be produced by heat treatment. As it was mentioned in eq 5, Na_2CO_3 undergoes decomposition into metastable Na_2O and CO_2 at elevated temperatures. Since Na is in the form of a metastable phase, it takes the phosphate from ScP and produces Na_3PO_4 and consequently forms one of the targeted phases, $NaScO_2$. On the other hand, the greater proportion of the ScP was transformed into again $Na_3Sc_2(PO_4)_3$ due to high temperature processing. As was revealed by DTA analysis of ScP (Figure 1c), ScP transforms into pyrophosphate at high temperatures. Formation of the pyrophosphate phases could be one of the major reasons why ScP is still presented as $Na_3Sc_2(PO_4)_3$, which is a relatively more stable phase at high temperatures. Although the removal of the phosphate moiety was unsuccessful, this process could be an alternative for the production of $Na_3Sc_2(PO_4)_3$, aka Sc NASICON which has enhanced photoluminescence properties.[31,32]

The reactions between ScP and high T_m Na compounds could be written as follows:

$$4Sc_9(HPO_4)_{10}(H_2PO_4)_5(OH)_2{\cdot}27H_2O + 54NaCl \xrightarrow{900\,^\circ C} 18Na_3Sc_2(PO_4)_3 + 3P_2O_5 + 54HCl(g) + 125H_2O(g) \quad (6)$$

$$4Sc_9(HPO_4)_{10}(H_2PO_4)_5(OH)_2{\cdot}27H_2O + 27Na_2SO_4 \xrightarrow{900\,^\circ C} 18Na_3Sc_2(PO_4)_3 + 3P_2O_5 + 27SO_3(g) + 152H_2O(g) \quad (7)$$

DOI: 10.1021/acs.iecr.9b02411
Ind. Eng. Chem. Res. XXXX, XXX, XXX−XXX

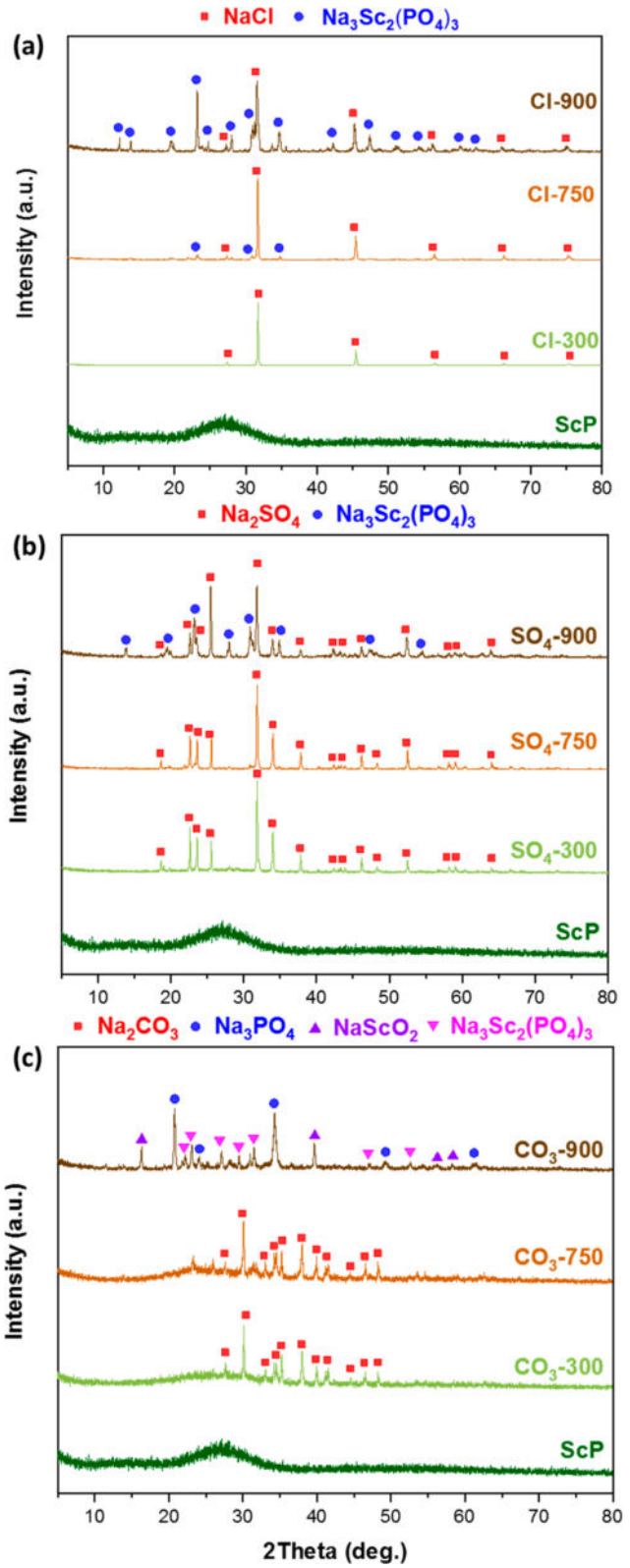

Figure 2. Powder XRD of the solid-state ScP conversion samples using NaCl (a), Na_2SO_4 (b), and Na_2CO_3 (c).

$$4Sc_9(HPO_4)_{10}(H_2PO_4)_5(OH)_2\cdot 27H_2O + 27Na_2O \xrightarrow{900\ ^\circ C} 18Na_3Sc_2(PO_4)_3 + 3P_2O_5 + 152H_2O(g) \quad (8)$$

It can be judged from these findings that in order to convert ScP into phosphate-free Sc compounds, lower processing temperatures should be used. In addition, to trigger the transformation by diffusion, the reacting Na compounds should not be stable at the processing temperatures. Therefore, low T_m Na compounds could be the best candidates to produce Na_3PO_4 and transform ScP completely, since diffusion would be easier in a melt and Na_3PO_4 would be the most stable compound during reaction.

As a verification of phases found in the XRD diffractogram, the SEM micrographs after high temperature treatment of ScP with high T_m Na compounds are illustrated in Figure 3. In all cases, the diffusion of Na into ScP structure to form monoclinic $Na_3Sc_2(PO_4)_3$ is observed and verified by EDX measurements. It can be seen from Figure 3a that the formed $Na_3Sc_2(PO_4)_3$ particles surround the surface of the unreacted cubic NaCl particles. A very similar case is also shown in Figure 3b where ScP particles are ground together with Na_2SO_4 and heated to 900 °C. As a result of Na diffusion to ScP, reacted and converted ScP particles can be seen on the surface of unreacted Na_2SO_4. However, in the case of Na_2CO_3, some differences were noticed. As was shown in eq 5, Na_2CO_3 decomposes into Na_2O and the generation of CO_2 starts above 850 °C. The formation of CO_2 can be seen from Figure 3c as the remaining gas releases holes in the resulting structure. Consequently, the formed structure is very porous. Partly successful transformation is found in this case since metastable Na_2O phase is reacted to form more stable Na_3PO_4 phase by taking phosphate from the only available phosphate source, ScP.

Overall, high temperature treatment with high T_m Na compounds is not the best choice to remove the phosphate moiety from the synthesized ScP particles since $Na_3Sc_2(PO_4)_3$ phase is formed as a result of diffusion from the ionic melt during the treatment. In all cases, instead of a fine dispersion of particles, sintered particles with a porous structure were observed as a result of the high temperature heat treatment.

3.3. Solid-State Interaction between ScP and Low T_m Na Compounds (NaOH and $NaNO_3$). In the previous section, it was discussed that lower temperatures were needed to achieve complete transformation of ScP into a phosphate-free compound. For this purpose, two appropriate candidates, NaOH and $NaNO_3$, were selected for further investigation. NaOH was selected as one of the most promising candidates to convert ScP into oxide or mixed oxide because of its low melting temperature. NaOH is a strong base with a melting point of 318 °C and a boiling point of 1388 °C (eq 9). The second candidate showing the potential to successfully complete the transformation was chosen to be $NaNO_3$ as this compound melts in a similar temperature range like NaOH and undergoes decomposition yielding first $NaNO_2$ and O_2 and later Na_2O, N_2, and O_2 (eqs 10 and 11).[33]

$$NaOH(s) \xrightarrow{318\ ^\circ C} NaOH(l) \xrightarrow{1388\ ^\circ C} NaOH(g) \quad (9)$$

$$NaNO_3(s) \xrightarrow{308\ ^\circ C} NaNO_3(l) \xrightarrow{600\ ^\circ C} NaNO_2(l) + \frac{1}{2}O_2(g) \quad (10)$$

$$4NaNO_2(l) \xrightarrow{750\ ^\circ C} 2Na_2O(s) + 2N_2(g) + 3O_2(g) \quad (11)$$

These Na compounds were coupled with ScP and heated up to 1000 °C in DTA to observe the mass changes and the behavioral variations from pure ScP, and the thermograms are presented in Figure 4.

DOI: 10.1021/acs.iecr.9b02411
Ind. Eng. Chem. Res. XXXX, XXX, XXX−XXX

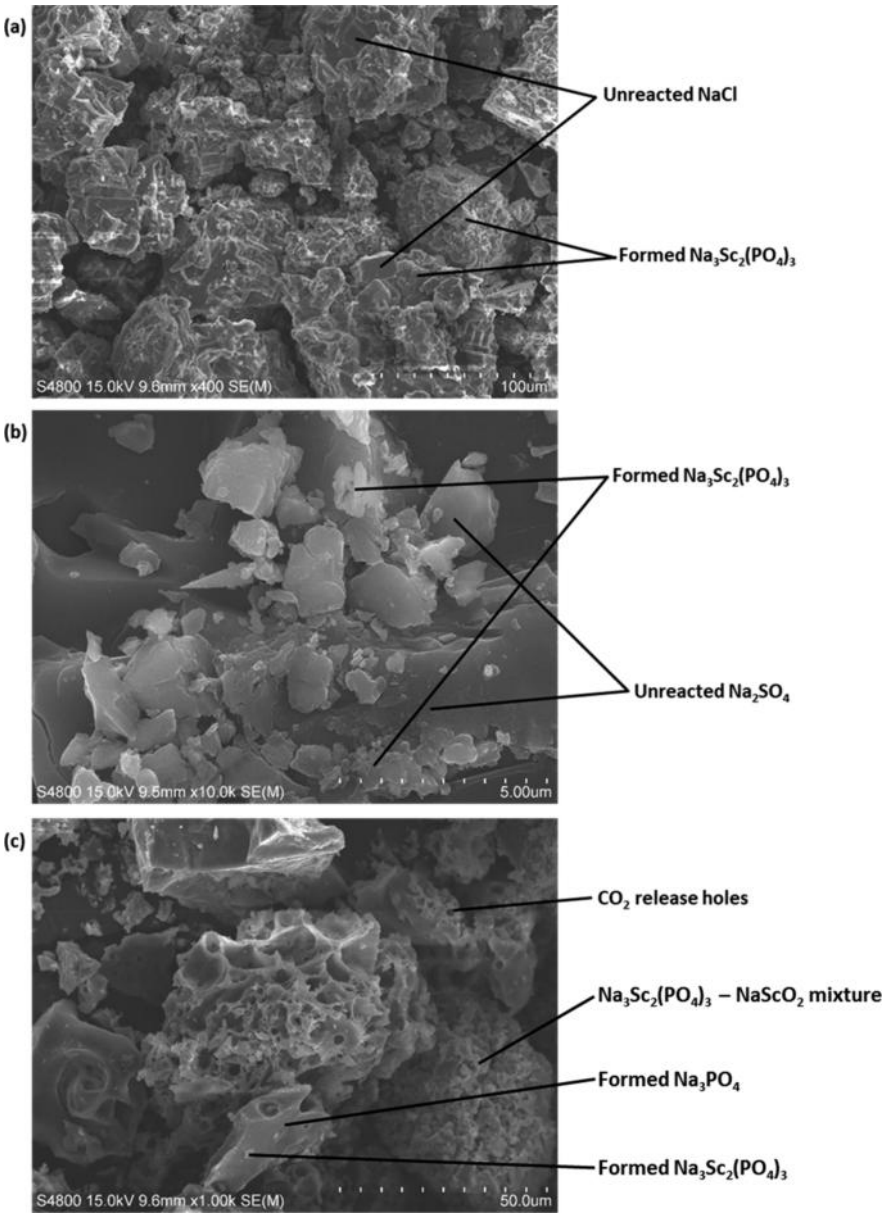

Figure 3. SEM micrographs of the conversion product for the samples Cl-900 (a), SO_4-900 (b), and CO_3-900 (c).

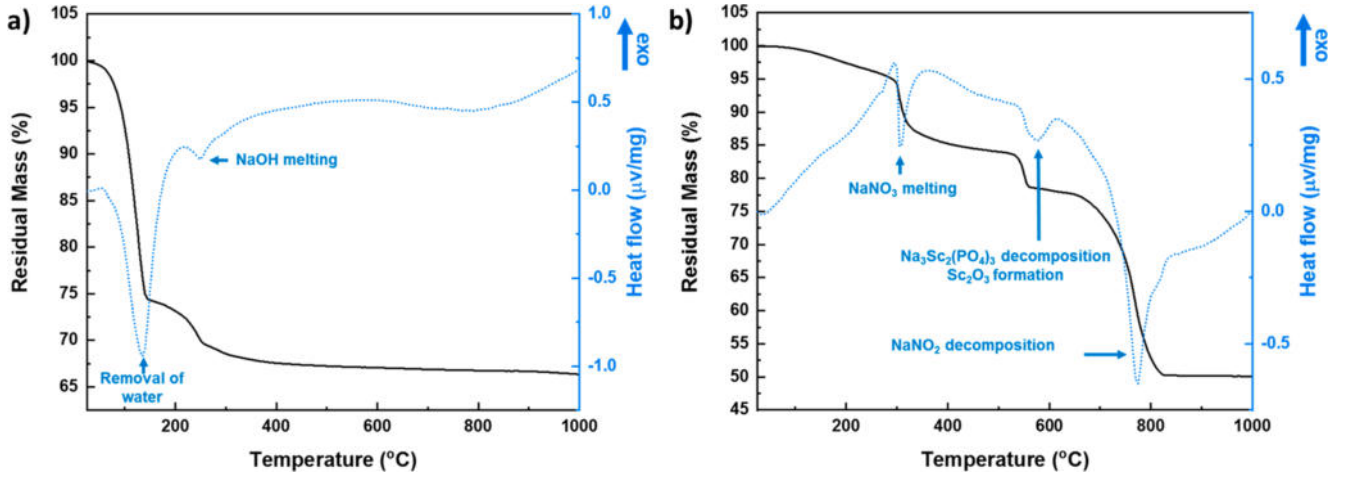

Figure 4. DSC-TGA measurements of (a) ScP + NaOH and (b) ScP + $NaNO_3$.

DOI: 10.1021/acs.iecr.9b02411
Ind. Eng. Chem. Res. XXXX, XXX, XXX−XXX

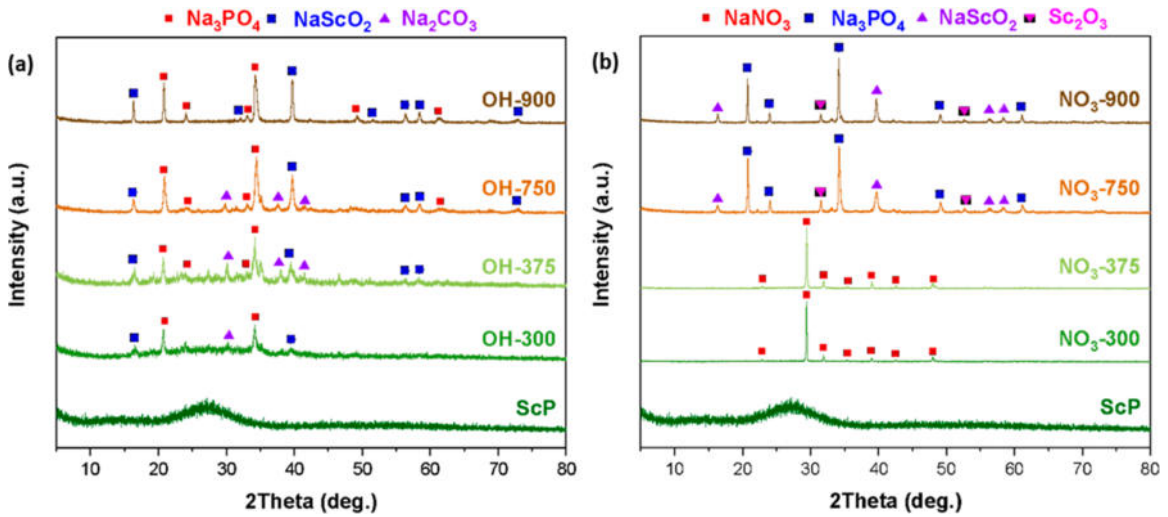

Figure 5. Powder XRD of the solid-state ScP conversion samples using NaOH (a) and $NaNO_3$ (b).

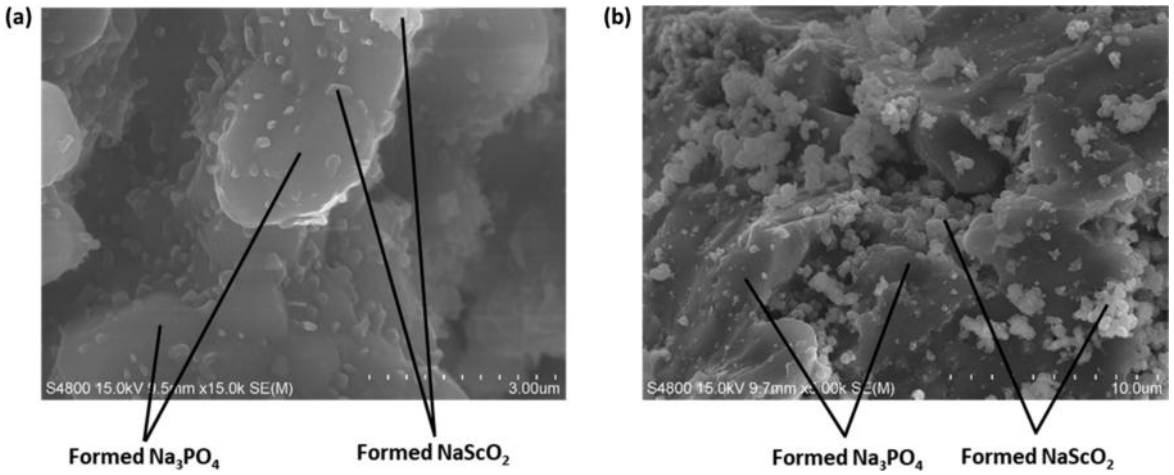

Figure 6. SEM micrographs showing the conversion product for the samples OH-900 (a) and NO_3-900 (b).

Some major differences were observed between the DSC-DTA of pure ScP (Figure 1c) and mixture of ScP−NaOH (Figure 4a). The first peak which reaches a maximum at 135 °C was characterized as the evaporation of physically and chemically bound water from both ScP and NaOH. Then NaOH started to melt at around 300 °C. While all of those mentioned peaks indicate some physical changes of the system, the condensation of HPO_4 and H_2PO_4 and the formation of the pyrophosphate were not detected in this thermogram as it was observed in the pure ScP sample. This is the first indication of successful conversion of ScP, while further characterization of the mechanism of the conversion needed investigation.

Similar to the NaOH case, the DSC thermogram that is obtained from coupled ScP-$NaNO_3$ (Figure 4b) showed greater variations than the pure ScP. First significant mass loss was observed when $NaNO_3$ started to melt at 308 °C. Since the melt of $NaNO_3$ is an ionic molten salt as NaOH, it immediately starts to react with the HPO_4 and OH groups in ScP and forms HNO_3. The HNO_3 formed is not thermally stable and decomposes into H_2O, NO_2, and O_2 at that temperature.[34] Although the condensation of HPO_4 and H_2PO_4 was not detected directly, it could be overlapped with the melting peak. As the temperature increases, $NaNO_3$ decomposes into $NaNO_2$ and releases O_2. As can be seen in the thermogram, a mass change was observed to occur at 550 °C which is suspected to be the decomposition of an intermediate metastable phase to yield Sc_2O_3. Around 750 °C, where the biggest mass change was observed, $NaNO_2$ decomposes into Na_2O and releases both N_2 and O_2. The major difference in behaviors between NaOH and $NaNO_3$ is the formation of the intermediate compound during conversion. The formation of this intermediate compound has an impact on the conversion mechanism and the resulted products.

A larger batch of ScP conversion was held while noting the mass changes from the samples collected at different temperatures, 300, 375, 750, and 900 °C, and the change in phases formed at the different heat treatment temperatures was characterized by powder XRD. The XRD diffractograms of the samples reacted with NaOH and $NaNO_3$ at different temperatures, and the phases found are shown in Figure 5a and Figure 5b.

Both the ScP and NaOH appear as amorphous phases at room temperature. Due to the caustic nature of NaOH, already when being heated at below the melting point of NaOH, conversion started. According to the Figure 5a, phases such as sodium phosphate (Na_3PO_4), sodium carbonate (Na_2CO_3),

DOI: 10.1021/acs.iecr.9b02411
Ind. Eng. Chem. Res. XXXX, XXX, XXX−XXX

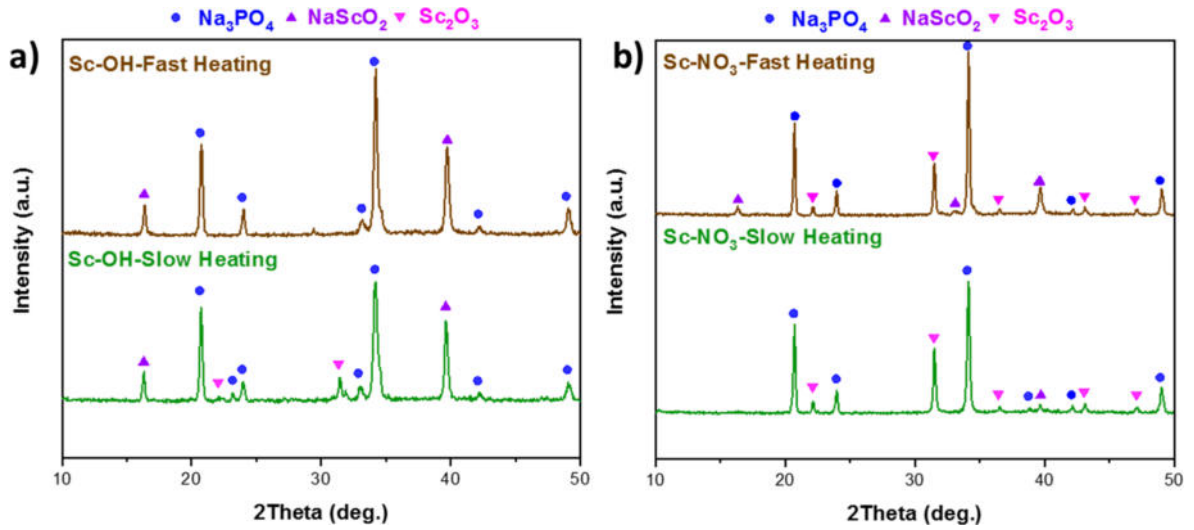

Figure 7. XRD diffractograms of (a) ScP-NaOH and (b) ScP-$NaNO_3$ showing the phase changes in different heating rates.

and sodium scandate ($NaScO_2$) were identified from the OH-300 sample. It is important to note that the reaction was conducted in an ambient atmosphere that contains CO_2. Further increase in reaction temperature liquefied NaOH and improved the conversion kinetics, while the identifiable phases remained practically the same. The only deviation is that Na_2CO_3 phase disappeared in the OH-900 sample, which is due to its thermal decomposition. Solid-state conversion of ScP by NaOH afforded $NaScO_2$ and Na_3PO_4, which successfully separated the Sc and P moieties.

Similar interaction was also observed when ScP was reacted with $NaNO_3$ as shown in Figure 5b. As expected, no stable phase other than $NaNO_3$ was detected at temperatures below 600 °C. However, as the temperature increased above the decomposing temperature of $NaNO_3$ (yielding $NaNO_2$ as well as releasing O_2), a diffusion controlled reaction was initiated. As it can be seen from the NO_3-750 sample, all of $NaNO_3$ was decomposed and formed Na_3PO_4 by exchanging Na and O with ScP. Different from the case of reaction with NaOH, as a result of O_2 release during decomposition, excess oxygen was introduced into the reaction and one of the most stable oxide phase of Sc, Sc_2O_3, is formed together with $NaScO_2$.

To understand the effect of the reaction on the products, the morphology of the samples treated at 900 °C was also investigated by SEM and those micrographs were presented in Figure 6. The $NaScO_2$ particles formed on the Na_3PO_4 can be clearly seen from Figure 6a. ScP particles were homogeneously dispersed on NaOH melt in the beginning which was followed by the initiation of the reaction. Therefore, fine $NaScO_2$ particles were identified directly on the formed Na_3PO_4. Similarly, P-free $NaScO_2$ can easily be detected by EDX measurements (see Supporting Information Figure S1) from Figure 6b as a result of the reaction between $NaNO_3$ and ScP. Although formed Sc_2O_3 could not be detected clearly in the EDX, the Sc mixed oxides can be detected and was shown in Figure 6b. Similar to the case for NaOH and Na compounds with higher T_m, diffusion reaction was again observed on the surface of the reactants. In this case complete conversion of P-free Sc compound was also verified by SEM and EDX, and this is contrary to the case of Na compounds with high T_m.

All of the findings presented up to now indicate that to remove the phosphate moiety completely from ScP and to form a mixed Sc oxide, low temperature processing is necessary. The main reasons behind this can be summarized as

(1) formation of pyrophosphate as the temperature increases above 750 °C which prevents the formation of $NaScO_2$,
(2) reaction through $Na_3Sc_2(PO_4)_3$ from ionic melt at high temperature conversion instead of $NaScO_2$,
(3) low stability of lower T_m Na compounds at lower temperatures due to instability of the melt, which catalyzes the transformation by diffusion.

Another important point to be noted is the formation of Sc_2O_3 at low temperatures. Although high heating rates were used for previous experiments, it is a promising result to form an almost complete Sc_2O_3 product since it is the most stable and desired Sc oxide. Contrary to the traditional route for Sc_2O_3 production, through calcination of $Sc_2(C_2O_4)_3$ above 750 °C, these low temperature conversion processes by lower T_m Na compounds can provide an alternative lower temperature Sc_2O_3 processing route when necessary time is given to complete the transformation reaction. Reactions between ScP and low T_m Na compounds yielding $NaScO_2$ or Sc_2O_3 could be written as the following.

Conversion reaction by NaOH:

$$Sc_9(HPO_4)_{10}(H_2PO_4)_5(OH)_2\cdot 27H_2O + 54NaOH \xrightarrow{375-900\ ^\circ C} 9NaScO_2 + 15Na_3PO_4 + 65H_2O(g) \quad (12)$$

Conversion reaction by $NaNO_3$, producing Sc_2O_3:

$$4Sc_9(HPO_4)_{10}(H_2PO_4)_5(OH)_2\cdot 27H_2O + 180NaNO_3 \xrightarrow{900\ ^\circ C} 18Sc_2O_3 + 60Na_3PO_4 + 90N_2(g) + 225O_2(g) + 76H_2O(g) \quad (13)$$

Conversion reaction by $NaNO_3$, producing $NaScO_2$:

$$2Sc_9(HPO_4)_{10}(H_2PO_4)_5(OH)_2\cdot 27H_2O + 108NaNO_3 \xrightarrow{900\ ^\circ C} 18NaScO_2 + 30Na_3PO_4 + 54N_2(g) + 135O_2(g) + 76H_2O(g) \quad (14)$$

3.4. Detailed Investigation of Conversion Process. The same conversion procedure was applied in different

DOI: 10.1021/acs.iecr.9b02411
Ind. Eng. Chem. Res. XXXX, XXX, XXX−XXX

heating rates to reproduce and prove that the formation of Sc_2O_3 is related to the kinetics of the solid state reaction.

Heating rate has a direct effect on formation of the Sc related phases (Figure 7). When NaOH and ScP are reacted in the oven with high heating rate, no Sc_2O_3 phase was found in the diffractogram as shown in Figure 7a. However, when the same operation was repeated with a slower heating rate, not only a $NaScO_2$ phase was formed but also the Sc_2O_3 was found in the converted product. Similarly, as was discussed in the previous section, the release of O_2 gas from $NaNO_3$ during decomposition favored the formation of Sc_2O_3. Although some minor $NaScO_2$ phase could still be identified from Figure 7b, the majority of the Sc-related phases were converted into Sc_2O_3 as a result of a slow heating rate. One of the most problematic element for Sc purification, Fe, was found as $NaFeO_2$ after conversion even at lower heating rates (see Supporting Information Figure S2). These findings show that the conversion products could be controlled easily with the heating rate of the process for both cases and the product synthesized could be selected according to the needs of further processing.

To understand the exact mechanism behind this conversion reaction, in situ XRD measurements were conducted. Variation of the phases with different temperatures could be seen from Figure 8. Below the melting point of $NaNO_3$ (308 °C), no

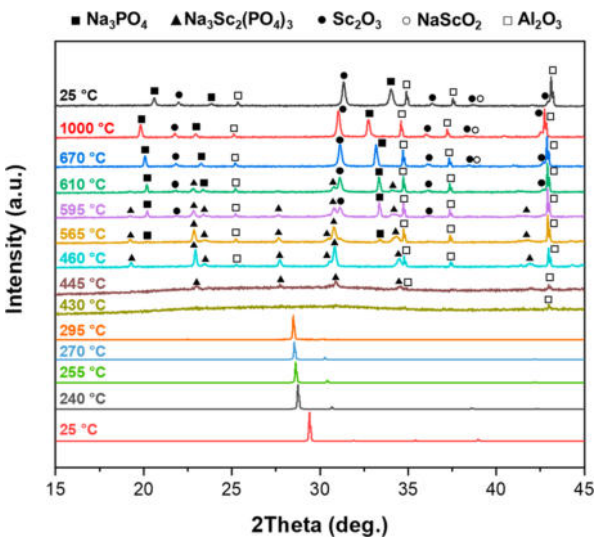

Figure 8. HTXRD patterns overlaid for monitoring the solid-state ScP conversion by $NaNO_3$.

crystalline phases other than the original $NaNO_3$ could be identified. When heated to 430 °C, all solid $NaNO_3$ completely melted and the conversion was initiated. Although the decomposition of $NaNO_3$ occurs at 600 °C, as an outcome of a continuous interaction between the molten $NaNO_3$ and the ScP, intermediate $Na_3Sc_2(PO_4)_3$, as identified in DSC before, was formed between 430 and 565 °C. However, this metastable intermediate structure is decomposed further into more stable Sc_2O_3 and Na_3PO_4 as the temperature is increased even further. Upon reaching 600 °C, only minor $Na_3Sc_2(PO_4)_3$ remained and the Sc-based phase is found majorly as Sc_2O_3.

The formation of this intermediate phase is the major difference in mechanism between successful conversion by NaOH and $NaNO_3$. The formation of NASICON Sc, which has very high ion conductivity, allowed ions to move easily[35−37] and favored the formation of Sc_2O_3 as soon as $NaNO_3$ melt started to decompose around 600 °C and provided additional O_2 to the system. This could also explain the reason why minor Sc_2O_3 formation was observed in the case of NaOH and the major portion of Sc was found as $NaScO_2$.

Note that the presence of Al_2O_3 was observed at temperatures above 460 °C, and this is because of the cracking of sample pellets that exposed partially the alumina crucible surface. There are practically no changes observed from XRD patterns after heating above 670 °C except thermal expansion and contraction. The final product that cooled back at room temperature exhibited a clear diffraction pattern consisting of Na_3PO_4, Sc_2O_3, and minor $NaScO_2$ phases. Since the heating rate of this measurement was very slow (2 °C/min), the most stable phases occurred after sufficient time had elapsed. As was discussed before, the use of low T_m Na compounds resulted in low temperature formation of Sc_2O_3 which could be implemented in industry as an alternative to Sc_2O_3 production without the use of an organic acid (oxalic acid).

3.5. Proof-of-Concept Demonstration on an Industrially Sourced Mixed Phosphate Sample. As was indicated in the previous section, the control of the Sc-based phases during the conversion operation could result in different uses in Sc processing. Sc is often sourced from industrial byproducts. It has been shown in recent years that certain types of bauxite residue contain exploitable amount of Sc.[15] A combined pyro- and hydrometallurgical approach was envisioned for multimetal recovery.[26,27,29] Through reductive smelting, Sc was concentrated into the slag phase. Slag leaching and subsequent selective phosphate precipitation produced a mixed phosphate salts where Sc was concentrated. Notably, the major composition of such mixed phosphate sample was still aluminum phosphate (Table 1), while other multivalent cationic impurities were silicon, titanium, calcium, and iron, among others. The content of such mixed phosphate is assumed to be complicated, with the metals presenting as oxo- and hydroxylphosphate and (di)hydrogen phosphates. Silicon is most likely to be present in the form of silica due to the rise of solution pH during phosphate precipitation.

Here we have demonstrated that the solid-state reaction of ScP with $NaNO_3$ yielded direct formation of Sc_2O_3 with a slow heating rate. The conversion could therefore act as a purification step for the mixed phosphate sample if the resulting converted solids have different chemical dissolution behaviors. Since the predominant component in the mixed phosphate was aluminum phosphate, the powder XRD pattern (Figure 9) of the converted solids shows the distinctive reflections of sodium aluminate ($NaAlO_2$) and sodium phosphate (Na_3PO_4). Ilmenite ($FeTiO_3$) was formed as a result of the high-temperature conversion process. Silicon should remain as amorphous silica, and the contents of Ca and Sc were probably too low to warrant any in-house XRD phase identification.

In an ideal situation, silica and sodium aluminate should dissolve in alkaline solutions, while scandium oxide should not. This led us to examine the elemental dissolution of the converted solids. The converted oxide was leached six times with 1 M NaOH solution and then four times with 1 M HNO_3 solution. Almost all the elements of interest were dissolved after 10 cycles of leaching, and the detailed dissolution data are available in Supporting Information Table S1. The amount of

DOI: 10.1021/acs.iecr.9b02411
Ind. Eng. Chem. Res. XXXX, XXX, XXX−XXX

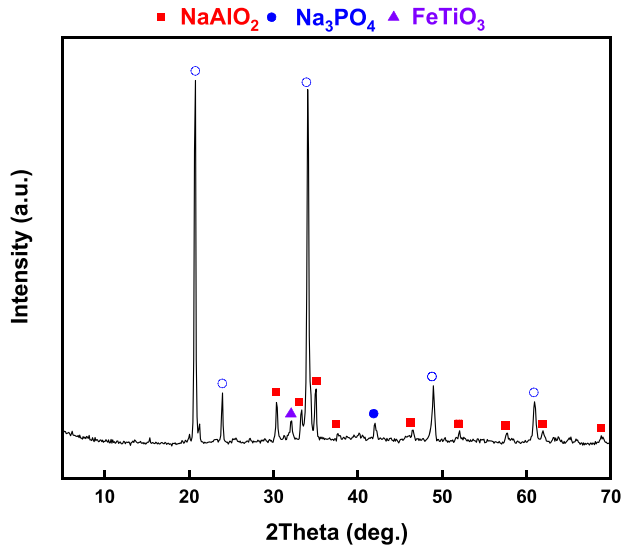

Figure 9. XRD diffractogram of the synthesized conversion product by reacting $NaNO_3$ and mixed phosphate sample.

dissolution of the elements in each cycle was given in Figure 10.

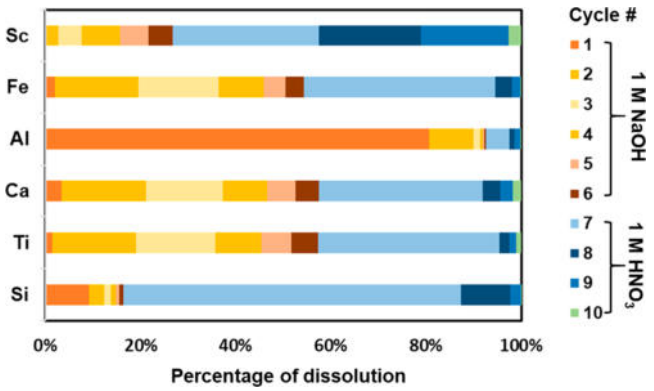

Figure 10. Dissolution percentages of the constituent elements in converted mixed phosphate in each washing cycle.

As shown in Figure 10, around 80% of the Al was dissolved immediately upon contacting with NaOH solution as expected due to high solubility of $NaAlO_2$ phase in alkali solutions. Therefore, major impurity in the phosphate precipitate is washed away with a negligible Sc loss. In order to test the dissolution behavior of the other impurities as well as the remaining Al, the same procedure was applied five more times. More than 90% of the Al was dissolved into solution with base leaching, while approximately 60% of Fe, Ca, and Ti were dissolved at the end of six alkali washing cycles. The alkalinity of 1 M NaOH seemed not sufficient enough for silica dissolution since merely 20% dissolved. Relatively small fraction of the total Sc (<30%) was leached in the basic condition and the remaining in the acid solution. By application of one cycle acid leaching after alkali washing, 90% or more of the impurities are dissolved and removed from the solid fraction while Sc loss stayed approximately around 55%. It was shown that almost all of the remaining impurities are soluble in acidic conditions while dissolution Sc_2O_3 kinetics were slower than the others. Therefore, the proposed solid-state conversion process would potentially serve as a purification step that could effectively eliminate alkaline/acid-soluble compounds with further optimization of the leaching/washing cycles.

Since the conversion was carried out in a furnace, the heating rate was not as low and as controlled as in the HTXRD case. Therefore, Sc-based phases could be still in the form of $NaScO_2$ and Sc_2O_3. That might be the reason why 30% Sc was dissolved as well in the end of alkali washing step. Although there are some significant Sc losses considering the value of Sc, almost 60% of all impurities were washed away only with alkali washing and the purity of the Sc product was enhanced immensely compared to the initial precipitate.

4. CONCLUSIONS

In this study, a solid-state conversion of ScP by using Na compounds was explored to remove the phosphate moiety from Sc. For this purpose, both high T_m Na compounds (NaCl, Na_2SO_4, and Na_2CO_3) and low T_m Na compounds (NaOH and $NaNO_3$) were tested. It was found that $Na_3Sc_2(PO_4)_3$ phase was formed instead of forming phosphate-free Sc compounds upon using high T_m Na compounds, and this is a result of mobilization of the Na ions from ionic melt in high temperature processing. Formation of pyrophosphates at higher temperatures and relatively higher stability of these Na compounds at high temperatures were found to be the cause behind unsuccessful conversion. Nevertheless, using high T_m Na salts for conversion could be an alternative to synthesize Sc NASICON with enhanced photoluminescence properties. On the other hand, ScP was successfully transformed into phosphate-free Sc compounds, $NaScO_2$ and Sc_2O_3, when low T_m Na compounds were used, because of the low thermodynamic stability of the melt in high temperatures. As a result of the lower temperature reaction, pyrophosphate formation was not observed in both cases.

Further investigations of the conversion process showed that the reaction products could be manipulated by controlling heating rate. Furthermore, it was found that complete Sc_2O_3 could be formed at lower temperatures than conventional processing temperatures as a result of slow heating rate. Hence, this conversion process could be a direct alternative for oxalic acid precipitation and successive calcination to produce Sc_2O_3. At the same time, one of the drawbacks of this conventional method, inclusion of organic content in the Sc_2O_3 product, could be completely avoided.

The conversion process was also tested for purification purposes using mixed phosphates synthesized from industrially sourced bauxite residue. After conversion with $NaNO_3$, Al and Fe phosphates yielded $Na(Al,Fe)O_2$ phases, while ScP was transformed into mixed $NaScO_2$ and Sc_2O_3. Alkali leaching of the converted product almost completely removed the Al, the major impurity in the mixture, as well as the 50% of the other impurities. Even though approximately 30% of the Sc was lost during this process, with proper upscaling and optimization this level could be further lowered. Therefore, this "P-to-O conversion" process could also serve as an intermediate purification operation or even a complete purification operation depending on the source material while removing the phosphate moiety from the product.

DOI: 10.1021/acs.iecr.9b02411
Ind. Eng. Chem. Res. XXXX, XXX, XXX−XXX

■ ASSOCIATED CONTENT

Supporting Information

The Supporting Information is available free of charge on the ACS Publications website at DOI: 10.1021/acs.iecr.9b02411.

EDX measurements after ScP-$NaNO_3$ conversion reaction (Figure S1), XRD diffractograms of FeP conversion process with varied heating rates (Figure S2), and dissolution percentages of the constituent elements in converted mixed phosphate sample in each cycle (Table S1) (PDF)

■ AUTHOR INFORMATION

Corresponding Author

*E-mail: bengi@meab-mx.com, bengiyagmurlu@gmail.com.

ORCID

Bengi Yagmurlu: 0000-0002-5376-1677
Wenzhong Zhang: 0000-0001-9184-0723
Risto T. Koivula: 0000-0002-6547-9775

Author Contributions

⊥B.Y. and W.Z. contributed equally to this paper.

Notes

The authors declare no competing financial interest.

■ ACKNOWLEDGMENTS

The research leading to these results has received funding from the European Community's Horizon 2020 Programme (H2020/2014−2019) under Grant Agreement 636876 (MSCA-ETN REDMUD). This publication reflects only the authors' view, exempting the Community from any liability. Project Web site is http://www.etn.redmud.org. The authors thank BAM (Bundesanstalt für Materialforschung und -prüfung) and Marie Hoffmann for their support in DSC measurements. Dr. Sami Hietala is gratefully acknowledged for solid-state NMR analysis.

■ REFERENCES

(1) UNFCCC. Adoption of the Paris Agreement. Report No. FCCC/CP/2015/L.9/Rev.1; http://unfccc.int/resource/docs/2015/cop21/eng/l09r01.pdf, 2015.

(2) Marquis, E.; Seidman, D. Nanoscale structural evolution of Al 3 Sc precipitates in Al (Sc) alloys. *Acta Mater.* **2001**, *49* (11), 1909−1919.

(3) Røyset, J.; Ryum, N. Scandium in aluminium alloys. *Int. Mater. Rev.* **2005**, *50* (1), 19−44.

(4) Lee, S.; Utsunomiya, A.; Akamatsu, H.; Neishi, K.; Furukawa, M.; Horita, Z.; Langdon, T. Influence of scandium and zirconium on grain stability and superplastic ductilities in ultrafine-grained Al−Mg alloys. *Acta Mater.* **2002**, *50* (3), 553−564.

(5) Seidman, D. N.; Marquis, E. A.; Dunand, D. C. Precipitation strengthening at ambient and elevated temperatures of heat-treatable Al (Sc) alloys. *Acta Mater.* **2002**, *50* (16), 4021−4035.

(6) Ormerod, R. M. Solid oxide fuel cells. *Chem. Soc. Rev.* **2003**, *32* (1), 17−28.

(7) Yamamoto, O. Solid oxide fuel cells: fundamental aspects and prospects. *Electrochim. Acta* **2000**, *45* (15), 2423−2435.

(8) Weber, A.; Ivers-Tiffée, E. Materials and concepts for solid oxide fuel cells (SOFCs) in stationary and mobile applications. *J. Power Sources* **2004**, *127* (1−2), 273−283.

(9) Gambogi, J. *USGS Minerals Information: Scandium*; U.S. Geological Survey, January 2017, 2018; pp 144−145.

(10) European Commision. Study on the review of the list of Critical Raw Materials: Executive Summary. Directorate-General for Internal Market, Industry, Entrepreneurship and SMEs, European Union, 2017; pp 1−93.

(11) Feuling, R. J. Recovery of scandium, yttrium and lanthanides from titanium ore. Patent US5049363A, 1991.

(12) Liu, Z.; Li, H. Metallurgical process for valuable elements recovery from red mud—A review. *Hydrometallurgy* **2015**, *155*, 29−43.

(13) Kaya, Ş.; Topkaya, Y. Extraction behavior of scandium from a refractory nickel laterite ore during the pressure acid leaching process. In *Rare Earths Industry*; Elsevier, 2016; pp 171−182.

(14) Horovitz, C. T. *Scandium Its Occurrence, Chemistry Physics, Metallurgy, Biology and Technology*; Elsevier, 2012.

(15) Borra, C. R.; Blanpain, B.; Pontikes, Y.; Binnemans, K.; van Gerven, T. Recovery of Rare Earths and Other Valuable Metals From Bauxite Residue (Red Mud): A Review. *Journal of Sustainable Metallurgy* **2016**, *2* (4), 365−386.

(16) Ditze, A.; Kongolo, K. Recovery of scandium from magnesium, aluminium and iron scrap. *Hydrometallurgy* **1997**, *44* (1−2), 179−184.

(17) Wang, W.; Cheng, C. Y. Separation and purification of scandium by solvent extraction and related technologies: a review. *J. Chem. Technol. Biotechnol.* **2011**, *86* (10), 1237−1246.

(18) Yagmurlu, B.; Dittrich, C.; Friedrich, B. Effect of Aqueous Media on the Recovery of Scandium by Selective Precipitation. *Metals* **2018**, *8* (5), 314.

(19) Zhang, W.; Avdibegović, D.; Koivula, R.; Hatanpää, T.; Hietala, S.; Regadío, M.; Binnemans, K.; Harjula, R. Titanium alkylphosphate functionalised mesoporous silica for enhanced uptake of rare-earth ions. *J. Mater. Chem. A* **2017**, *5* (45), 23805−23814.

(20) Zhang, W.; Koivula, R.; Wiikinkoski, E.; Xu, J.; Hietala, S.; Lehto, J.; Harjula, R. Efficient and selective recovery of trace scandium by inorganic titanium phosphate ion-exchangers from leachates of waste bauxite residue. *ACS Sustainable Chem. Eng.* **2017**, *5* (4), 3103−3114.

(21) Avdibegović, D.; Regadío, M.; Binnemans, K. Recovery of scandium (III) from diluted aqueous solutions by a supported ionic liquid phase (SILP). *RSC Adv.* **2017**, *7* (78), 49664−49674.

(22) Avdibegović, D.; Yagmurlu, B.; Dittrich, C.; Regadío, M.; Friedrich, B.; Binnemans, K. Combined multi-step precipitation and supported ionic liquid phase chromatography for the recovery of rare earths from leach solutions of bauxite residues. *Hydrometallurgy* **2018**, *180*, 229−235.

(23) Yagmurlu, B.; Dittrich, C.; Friedrich, B. Precipitation Trends of Scandium in Synthetic Red Mud Solutions with Different Precipitation Agents. *Journal of Sustainable Metallurgy* **2017**, *3* (1), 90−98.

(24) Wood, S. A.; Samson, I. M. The aqueous geochemistry of gallium, germanium, indium and scandium. *Ore Geol. Rev.* **2006**, *28* (1), 57−102.

(25) Travers, J. G.; Dellien, I.; Hepler, L. G. Scandium: Thermodynamic properties, chemical equilibria, and standard potentials. *Thermochim. Acta* **1976**, *15* (1), 89−104.

(26) Alkan, G.; Xakalashe, B.; Yagmurlu, B.; Kaussen, F.; Friedrich, B. Conditioning of red mud for subsequent titanium and scandium recovery−a conceptual design study. *World Metall.—Erzmet.* **2017**, *70* (2), 5−12.

(27) Alkan, G.; Yagmurlu, B.; Gronen, L.; Dittrich, C.; Ma, Y.; Stopic, S.; Friedrich, B. Selective silica gel free scandium extraction from Iron-depleted red mud slags by dry digestion. *Hydrometallurgy* **2019**, *185*, 266−272.

(28) Alkan, G.; Yagmurlu, B.; Cakmakoglu, S.; Hertel, T.; Kaya, Ş.; Gronen, L.; Stopic, S.; Friedrich, B. Novel Approach for Enhanced Scandium and Titanium Leaching Efficiency from Bauxite Residue with Suppressed Silica Gel Formation. *Sci. Rep.* **2018**, *8* (1), 5676.

(29) Yagmurlu, B.; Alkan, G.; Xakalashe, B.; Friedrich, B.; Stopic, S.; Dittrich, C. Combined SAF Smelting and Hydrometallurgical Treatment of Bauxite Residue for Enhanced Valuable Metal Recovery. Presented at ICSOBA-2017, 35th International Conference and Exhibition of ICSOBA, Germany, 2017.

DOI: 10.1021/acs.iecr.9b02411
Ind. Eng. Chem. Res. XXXX, XXX, XXX−XXX

(30) Schmutz, C.; Barboux, P.; Ribot, F.; Taulelle, F.; Verdaguer, M.; Fernandez-Lorenzo, C. EXAFS, Raman and 31P NMR study of amorphous titanium phosphates. *J. Non-Cryst. Solids* **1994**, *170* (3), 250−262.
(31) Guo, H.; Devakumar, B.; Li, B.; Huang, X. Novel Na3Sc2 (PO4) 3: Ce3+, Tb3+ phosphors for white LEDs: Tunable blue-green color emission, high quantum efficiency and excellent thermal stability. *Dyes Pigm.* **2018**, *151*, 81−88.
(32) Guo, H.; Huang, X.; Zeng, Y. Synthesis and photoluminescence properties of novel highly thermal-stable red-emitting Na3Sc2 (PO4) 3: Eu3+ phosphors for UV-excited white-light-emitting diodes. *J. Alloys Compd.* **2018**, *741*, 300−306.
(33) Freeman, E. S. The kinetics of the thermal decomposition of sodium nitrate and of the reaction between sodium nitrite and oxygen. *J. Phys. Chem.* **1956**, *60* (11), 1487−1493.
(34) Robertson Jr, G. D.; Mason, D. M.; Corcoran, W. H. The kinetics of the thermal decomposition of nitric acid in the liquid phase. *J. Phys. Chem.* **1955**, *59* (8), 683−690.
(35) Susman, S.; Delbecq, C.; Brun, T.; Prince, E. Fast ion transport in the NASICON analog Na3Sc2 (PO4) 3: Structure and conductivity. *Solid State Ionics* **1983**, *9*, 839−844.
(36) Tamura, S.; Imanaka, N.; Adachi, G. y. Trivalent Sc3+ Ion Conduction in Sc1/3Zr2 (PO4) 3 Solids with the NASICON-Type Structure. *Adv. Mater.* **1999**, *11* (18), 1521−1523.
(37) Anantharamulu, N.; Rao, K. K.; Rambabu, G.; Kumar, B. V.; Radha, V.; Vithal, M. A wide-ranging review on Nasicon type materials. *J. Mater. Sci.* **2011**, *46* (9), 2821−2837.

DOI: 10.1021/acs.iecr.9b02411
Ind. Eng. Chem. Res. XXXX, XXX, XXX−XXX